Opto-Electronic Advances

CN 51–1781/TN ISSN 2096–4579 (Print) ISSN 2097–3993 (Online)

Flicker minimization in power-saving displays enabled by measurement of difference in flexoelectric coefficients and displacement-current in positive dielectric anisotropy liquid crystals

Junho Jung, HaYoung Jung, GyuRi Choi, HanByeol Park, Sun-Mi Park, Ki-Sun Kwon, Heui-Seok Jin, Dong-Jin Lee, Hoon Jeong, JeongKi Park, Byeong Koo Kim, Seung Hee Lee and MinSu Kim

Citation: Jung JH, Jung HY, Choi GR, et al. Flicker minimization in power-saving displays enabled by measurement of difference in flexoelectric coefficients and displacement-current in positive dielectric anisotropy liquid crystals. *Opto-Electron Adv* **8**, 250022(2025).

https://doi.org/10.29026/oea.2025.250022

Received: 12 February 2025; Accepted: 30 June 2025; Published online: 27 August 2025

Related articles

Dynamic interactive bitwise meta-holography with ultra-high computational and display frame rates
Yuncheng Liu, Ke Xu, Xuhao Fan, Xinger Wang, Xuan Yu, Wei Xiong, Hui Gao
Opto-Electronic Advances 2024 **7**, 230108 doi: 10.29026/oea.2024.230108

Multi-dimensional multiplexing optical secret sharing framework with cascaded liquid crystal holograms
Keyao Li, Yiming Wang, Dapu Pi, Baoli Li, Haitao Luan, Xinyuan Fang, Peng Chen, Yanqing Lu, Min Gu
Opto-Electronic Advances 2024 **7**, 230121 doi: 10.29026/oea.2024.230121

More related article in Opto-Electronic Journals Group website

OEA Opto-Electronic Advances

http://www.oejournal.org/oea

OE_Journal @OptoElectronAdv

Opto-Electronic Advances

Article

September 2025, Vol. 8, No. 9

DOI: 10.29026/oea.2025.250022 CSTR: 32247.14.oea.2025.250022

Flicker minimization in power-saving displays enabled by measurement of difference in flexoelectric coefficients and displacement-current in positive dielectric anisotropy liquid crystals

Junho Jung[1,2], HaYoung Jung[3], GyuRi Choi[3], HanByeol Park[3], Sun-Mi Park[4], Ki-Sun Kwon[4], Heui-Seok Jin[4], Dong-Jin Lee[2], Hoon Jeong[2], JeongKi Park[2], Byeong Koo Kim[2], Seung Hee Lee[1,3,5]* and MinSu Kim[3]*

Balancing high display performance with energy efficiency is crucial for global sustainability. Lowering operating frequencies—such as enabling 1 Hz operation in fringe-field switching (FFS) liquid crystal displays—reduces power consumption but is hindered by image flicker. While negative dielectric anisotropy liquid crystals (nLCs) mitigate flicker, their high driving voltages and production costs limit adoption. Positive dielectric anisotropy liquid crystals (pLCs) offer lower operating voltages, faster response times, and broader applicability, making them a more viable alternative. This study introduces a novel approach to minimizing flexoelectric effects in pLCs by investigating how single components influence flexoelectric behavior in mixtures through an effective experimental methodology. Two innovative measurement techniques—(1) flexoelectric coefficient difference analysis and (2) displacement-current measurement (DCM)—are presented, marking the first application of DCM for verifying flexoelectric effects. The proposed system eliminates uncertainties associated with previous methods, providing a reliable framework for selecting liquid crystal components with minimal flexoelectric effects while preserving key electro-optic properties. Given pLCs' higher reliability, lower production costs, and broader material selection, these advancements hold significant potential for low-power displays. We believe this work enhances flexoelectric analysis in nematic liquid crystals and contributes to sustainable innovation in the display industry, aligning with global energy-saving goals.

Keywords: low power displays; various refresh rate; flexoelectric effect; flicker; fringe-field switching (FFS); liquid crystal displays (LCDs)

Jung JH, Jung HY, Choi GR et al. Flicker minimization in power-saving displays enabled by measurement of difference in flexoelectric coefficients and displacement-current in positive dielectric anisotropy liquid crystals. *Opto-Electron Adv* **8**, 250022 (2025).

[1]Dept. of Polymer Nano Science and Technology, Jeonbuk National University, Jeonju, Jeonbuk 54896, Korea; [2]LG Display Co., Ltd., Paju, Gyeonggi 10845, Korea; [3]Dept. of Nano Convergence Engineering, Jeonbuk National University, Jeonju, Jeonbuk 54896, Korea; [4]Merck Performance Materials Ltd., Pyeongtaek, Gyeonggi 17956, Korea; [5]Dept. of JBNU-KIST Industry-Academia Convergence Research, Jeonbuk National University, Jeonju, Jeonbuk 54896, Korea.

*Correspondence: SH Lee, E-mail: lsh1@jbnu.ac.kr; MS Kim, E-mail: minsu.kim@jbnu.ac.kr

Received: 12 February 2025; Accepted: 30 June 2025; Published online: 27 August 2025

Open Access This article is licensed under a Creative Commons Attribution 4.0 International License.
To view a copy of this license, visit http://creativecommons.org/licenses/by/4.0/.

© The Author(s) 2025. Published by Institute of Optics and Electronics, Chinese Academy of Sciences.

Introduction

In the display industry, technologies aimed at reducing power consumption have become increasingly essential in response to global energy-saving policies[1,2]. Several approaches have been developed to address this demand, including inversion techniques[3], dynamic backlight control[4], and variable frame refresh rates[5]. In particular, reducing the refresh rate of a display panel leads to significant power savings, primarily because dynamic power consumption is proportional to both the switching frequency and the capacitive load in the thin-film transistor (TFT) array. Among these strategies, the flexoelectric effect in liquid crystal displays (LCDs) has garnered attention due to its notable impact on variable frame refresh rate performance[6–8]. Flexoelectricity arises from spatial strain gradients within mesogenic LCs[9–11], causing light transmittance difference and flickering on a display at low refresh rates. This phenomenon occurs due to uneven electric fields between frames of alternating current (AC) voltage and flexoelectric contribution in LC deformation between the electrodes over time.

The necessity for such advancements is underscored by the evolving demands of the display industry. While high refresh rate displays (e.g., 120 Hz, 144 Hz, 240 Hz) significantly enhance video playback and gaming experiences[12,13], they also incur substantially higher power consumption—typically two to three times more than traditional 60 Hz operation. In the context of global energy efficiency initiatives, this trade-off between performance and energy use is becoming increasingly unsustainable. There is a growing need for display technologies capable of supporting a broad range of refresh rates—from as low as 1 Hz to as high as 240 Hz—to dynamically adapt to different content types and optimize power consumption accordingly. Although a significant portion of power consumption in LCDs originates from the backlight unit, particularly in LED-based systems[14–16], implementing ultra-low-frequency driving (e.g., 1 Hz) can substantially reduce energy use during static or low-motion content. Furthermore, integrating such low-frequency operation with dynamic refresh rate modulation—allowing automatic switching between different modes based on content demand—represents a promising direction for next-generation energy-efficient displays. This combined approach is expected to become increasingly important and even essential in future display technologies.

Achieving low refresh rates in LCDs while mitigating flicker has been a significant challenge. Previous methods, including the use of symmetric electric fields, manipulation of LC physical properties, and a deeper understanding of the flexoelectric effect, have often fallen short in fully eliminating flicker while maintaining image qualities. Predicting the flexoelectric effect and measuring the flexoelectric constants have been scientifically interesting but practically challenging due to the complexity of measurement techniques, other factors such as ion impurity effects, errors in measuring the surface anchoring strengths of vertical and planar alignments, the involvement of twist deformation, and the consistency in formation of an electric field with actual fringe-field switching (FFS) mode[17–19]. Consequently, commercially viable flicker-free 1 Hz displays have been rarely produced. We successfully interpreted and understood the flexoelectric phenomenon, developing a straightforward method to measure the difference in flexoelectric coefficients (e_s–e_b); e_s and e_b denote splay and bend flexoelectric coefficients, respectively. Kim et al. reported that their industry-academia collaboration team achieved a milestone by prototyping the world's first flicker-free 1 Hz-refresh-rate 13.4-inch (1 inch = 2.54 cm) WUXGA FFS-LCD on a laptop platform using negative dielectric anisotropy LCs (nLCs)[20]. The core of this research lies in predicting (e_s–e_b) values for different LCs by matching the measured transmittance differences between altering frames of AC electric signals with simulated results in cells which are identical to the FFS cell structure but vertically aligned LC. In this system, applying electric fields below the threshold that induces discontinuous LC alignment effectively suppresses twist deformation. This enables the isolation and accurate measurement of pure splay and bend deformations. Because twist deformation is eliminated, the applied electric energy is not dissipated through twisting, allowing the observed brightness to be directly attributed to splay and bend deformations associated with flexoelectric polarization (Fig. S1)[21]. This approach enabled us to identify LCs that minimize flickers while maximizing electro-optic performance and successfully implementing these findings in real products.

Yet, while the nLCs provide higher transmittance, they inherently have higher driving voltages, higher manufacturing cost, and slower response time, compared to positive dielectric anisotropy LCs (pLCs)[22]. The molecular structure of nLCs inherently limits the reduction of driving voltage, and their high viscosity leads to slower response times and challenges in optimizing retardation settings. These factors limit their application in many products beyond high-end devices. This work focuses on predicting and gauging the flexoelectric coefficient difference in pLCs, and we aim to provide a viable alternative that offers fast response time, low driving voltages, and low cost for manufacturing, which expand the potential for low-refresh rate products for ultralow power displays. Our study addresses the effective measurement method and results for energy-efficient display solutions by focusing on reducing flicker at low-refresh rates in pLCs. This advancement represents a significant step towards achieving both high performance and sustainability goals in display technology, paving the way for a more energy-conscious future.

Although the proposed flexoelectric coefficient difference measurement system on nLC was successful, this system on pLC requires deeper understanding on how the flexoelectric effect involves in the measurement system and the practical system. To minimize flicker, it is easy to imagine that the flexoelectric effect should be eliminated as earlier stages of works[21,23–26]. However, more important point we anticipate in this stage is how the spatially averaged optical appearance (within the spatial resolving power of human eyes) would be in the similar level over the AC frames in time. Knowing each splay or bend flexoelectric coefficient limits to provide sufficient information from this perspective. Thus, we used the same FFS electrode structures with identical electric field formation for deriving the flexoelectric coefficient difference. The nematic LC director field analysis from the vertically aligned FFS cell proves the importance of the flexoelectric coefficient difference. The spatially modulating flexoelectric contribution, which would be temporally averaged out for the optical appearance, provides the splay and bend flexoelectric contributions in nLC and pLC are in a similar tendency even if their reorientation upon dielectric coupling is obviously different. We also verified the flexoelectric contribution and ion impurity level in pLC system by a commercially available displacement-current measurement (DCM) method for the first time in this field[27].

This result gives rise to the simplicity when employing negative or positive LC into the actual FFS cell structure. In addition, based on this understanding we were able to choose which of single LC molecules would be the best for the appropriate mixture for reduction in image flickers. We thus verified that the newly proposed mixture showed minimum flexoelectric coefficient difference, measured from the vertically aligned FFS cell. And we demonstrated the minimum temporal transmittance difference for lowest flicker in planarly-aligned normal FFS cells. We believe that this result will expand the applicability of this system for ultralow power consumption displays to meet with global energy saving efforts.

Experimental section

Materials: We firstly verified the flexoelectric effect in an FFS cell with positive LC (pLC0, Δn = 0.078, Merck) for measuring transmittance difference between AC frames. Based on the analysis of the transmittance difference, we varied concentration of different singles with different dielectric anisotropy, and three different LC mixtures (pLC1, pLC2, pLC3) were examined. The mixtures were purified to reduce ion impurities. We combined singles with dipole moment perpendicular to the molecule's long axis and neutral molecules, which determine dipoles and quadrupoles, respectively, as detailed in Table 1. The optimization of the ratio K_{33}/K_{11} could lead to the suppression of T_{diff}. However, the general description gives that each K_{11} and K_{33} influences the flexoelectric coefficients; for example, increasing K_{33} could also increase in e_b. This is in a trade-off relation. Investigation of flexoelectric coefficients based on the Helfrich model enabled us to avoid such trade-off relation although this method might be imperfect when applied to mixtures of LCs with different types of constituents. Flexoelectric polarization is described by the equation $\boldsymbol{P}_f = e_s\boldsymbol{n}(\nabla\cdot\boldsymbol{n}) + e_b\boldsymbol{n}\times(\nabla\times\boldsymbol{n})$, where e_s and e_b represent the splay and bend flexoelectric coefficients, respectively[6,11,21]. A statistical model proposed by Helfrich provides a theoretical framework for estimating e_s and e_b based on molecular packing, dipole moments, and elastic constants. According to this model, the coefficients are given by $e_s = \delta\left(\frac{a}{b}\right)^{\frac{1}{3}} N^{\frac{1}{3}}\left(\frac{2\boldsymbol{\mu}_{\parallel}K_{11}}{k_BT}\right)$ and $e_b = \delta\left(\frac{b}{a}\right)^{\frac{2}{3}} N^{\frac{1}{3}}\left(\frac{\boldsymbol{\mu}_{\perp}K_{33}}{2k_BT}\right)$, where a and b are the major and minor axes of the approximated ellipsoidal molecules, and δ is the molecular kink angle. Here, $\boldsymbol{\mu}_{\parallel}$ and $\boldsymbol{\mu}_{\perp}$ denote the dipole moments parallel and perpendicular to the molecular long axis, K_{11} and K_{33} are the splay and bend elastic constants, k_B is the Boltzmann constant, T is the temperature, and N is the molecular number density[9,28,29]. In designing our LC mixtures, we carefully controlled the concentrations of individual components, including neutral single molecules, to optimize the flexoelectric properties while meeting the physical requirements for high-performance display operation. For each constituent molecule, key parameters such as molecular shape, dipole moment, dielectric anisotropy, and elastic constants were independently considered for their influence on the overall flexoelectric coefficients of the mixture. The concentration ratios of the three representative constituents —C1 (high-polar), C2 (mid-polar), and C3 (neutral)—used in each pLC formulation are summarized in Table 1.

As shown in Table 1, pLC1 exhibits a relatively higher measured value of ($e_s - e_b$) at compositions $c_1 = \alpha$, $c_2 = \beta$, $c_3 = \eta$. Initially, we hypothesized that reducing the number of single-component molecules would lower the flexoelectric coefficients. This expectation was based on the assumption that removing molecules with dipole moments poorly aligned with their major molecular axis would degrade packing efficiency, thereby reducing the molecular number density N. This trend was partially confirmed, as the measured ($e_s - e_b$) for pLC2 (which excludes component C2) was lower than that of pLC1. However, the reduction was not as significant as anticipated. Further analysis revealed that component C1 possesses a higher molecular aspect ratio (a/b) and greater rigidity compared to the other two components. These properties enhance molecular packing and contribute to a higher effective N, which in turn increases ($e_s - e_b$). In pLC3, where c_1 was reduced to 0.5α (with a corresponding increase in c_2 to maintain a sufficient dielectric anisotropy $\Delta\varepsilon$), the combined effects of decreased aspect ratio and reduced packing density led to a more pronounced decrease in the measured ($e_s - e_b$) as shown in Table 1.

Cell preparation: We fabricated two FFS cell types capable of inducing planar and vertical alignments. While the planarly aligned FFS cells are fabricated based on the representatives of normal FFS mode, the vertically aligned FFS (VA-FFS) cells, used to determine flexoelectric coefficients, consisted of patterned electrodes (electrode width w = 3.5 μm and distance l = 6 μm), an insulation layer, and plain electrodes with the cell gap d = 3.2 μm. Electrodes were made of indium tin oxide (ITO) via sputtering, while the insulation layer was produced from silicon nitride (SiN_x) via PECVD, provided by Merck. LC mixtures were injected into cells via capillary action.

Image acquisition: POM images (Eclipse LV100N POL, Nikon) were captured at 250 fps under an alternating current (AC) voltage at various frequencies, including 1 Hz, using a CCD camera (DS-Ri2, Nikon), a high-speed camera (Fastcam UX100, Photron Inc.), and an arbitrary function generator (AFG31021, Tektronix Inc.).

Electro-optic measurement: Voltages at various frequencies were applied to both planarly aligned and vertically aligned FFS cells using a waveform generator (AFG31021, Tektronix Inc.). These cells were placed between crossed polarizers, and illuminated with laser light from a He-Ne laser (λ = 633 nm). The transmitted light passing through the polarizers and the test cells was detected using a digital optical power meter (PM100D, Thorlabs Inc.) as shown in Fig. S2. By synchronizing the applied voltage waveforms with the detected optical signals, voltage- and time-dependent transmittance curves were obtained. The driving frequency was set to 1 kHz in the normal operation mode and 1 Hz in the flexoelectric measurement mode.

FEM simulation: Finite element method (FEM) simulations were performed using a multidimensional simulator (TechWiz LCD, Sanayi Systems) to analyze the electro-optical responses of the LC cells. The simulation considered the total free energy density of the system, comprising three key contributions: elastic, dielectric, and flexoelectric. The elastic free energy density was

Table 1 | Relative values of physical properties of liquid crystal (LC) mixtures with respect to the three representative constituents (C1, C2, and C3).

LC mixture	Δn [i]	$\Delta\varepsilon$ [ii]	γ_1 [iii] / [mPa·s]	K_{11} [iv] / [pN]	K_{33} [v] / [pN]	K_{33}/K_{11} [vi]	c_1 [vii] / [%]	c_2 [viii] / [%]	c_3 [ix] / [%]	$e_s - e_b$ [x] [pC/m]
pLC0	0.078	0.6e	2.9g	1.1u	1.5v	1.3w	-	-	-	-
pLC1	0.1086	e [xi]	g [xi]	u [xi]	v [xi]	w [xi]	α [xi]	β [xi]	η [xi]	2.5
pLC2	0.1095	1.2e	1.1g	1.0u	1.0v	1.0w	1.2α	-	1.0η	2.0
pLC3	0.1049	0.5e	1.0g	1.3u	1.2v	1.0w	0.5α	1.9β	1.2η	0.5

[i] Birefringence; [ii] Dielectric anisotropy; [iii] Rotational viscosity; [iv] Bend elastic constant; [v] Splay elastic constant; [vi] Ratio of bend to splay elastic constants; [vii] Concentration of constituent 1 (C1), high-polar; [viii] Concentration of constituent 2 (C2), mid-polar; [ix] Concentration of constituent 3 (C3), neutral; [x] Derived value of difference in splay and bend flexoelectric coefficients ($e_s - e_b$) based on the measurement and FEM simulation; [xi] These are constants and all other values are relative values to these. All mixtures contained low concentrations of additional constituents, which are not specified in this table.

defined as $f_{\text{elas}} = 1/2\left(K_{11}[\nabla\cdot\boldsymbol{n}]^2 + K_{22}[\boldsymbol{n}\cdot(\nabla\times\boldsymbol{n})]^2 + K_{33}[\boldsymbol{n}\times(\nabla\times\boldsymbol{n})]^2\right)$, where $\boldsymbol{n}$ is the director vector. The dielectric free energy density was expressed as $f_{\text{dielec}} = -1/2\varepsilon_0\Delta\varepsilon(\boldsymbol{n}\cdot\boldsymbol{E})^2$ and the flexoelectric coupling energy as $f_{\text{flexo}} = -[e_s\boldsymbol{n}(\nabla\cdot\boldsymbol{n}) + e_b\boldsymbol{n}\times(\nabla\times\boldsymbol{n})]\cdot\boldsymbol{E}$, where e_s and e_b are the splay and bend flexoelectric coefficients, respectively, and $\boldsymbol{E}$ is the electric field vector. The electric potential distribution within the LC cell was obtained by solving Laplace's equation. Optical transmittance and POM-like images were calculated using the extended [2×2] Jones matrix method. By systematically varying the flexoelectric coefficients in the simulation to match experimental results, we were able to indirectly determine the flexoelectric coefficient difference ($e_s - e_b$).

Displacement-current measurement (DCM): The current-voltage (*I*-*V*) characteristics of the LC layers in VA-FFS cells were measured using a DCM instrument (DCM1000, TOYOTech LLC). The degree of the flexoelectric effect was inferred from the symmetry of the *I*-*V* curves, particularly between the first and third quadrants of the *I*-*V* cycle. The equivalent circuit used for analysis is shown in Fig. S3. Each VA-FFS cell had the same electrode and insulating structure as the standard FFS cells and was filled with purified pLCs free of ionic impurities. Electrically, the LC cells behave as a parallel combination of a capacitor and resistor. A triangular waveform voltage was applied to generate *I*-*V* curves over three cycles at frequencies of 0.1 Hz, and 0.01 Hz. The total current I flowing through the LC layer is described by $I = I_C + I_R = C\frac{\mathrm{d}V}{\mathrm{d}t} + \frac{V}{R}$, where C is the capacitance, R is the resistance, and $\frac{\mathrm{d}V}{\mathrm{d}t}$ is the time derivative of the applied voltage. For $\frac{\mathrm{d}V}{\mathrm{d}t} > 0$ and $\frac{\mathrm{d}V}{\mathrm{d}t} < 0$, the current slopes are given as $I_p = C\frac{\mathrm{d}V}{\mathrm{d}t} + \frac{V}{R}$ and $I_n = -C\frac{\mathrm{d}V}{\mathrm{d}t} + \frac{V}{R}$, respectively. The difference between these slopes, $\Delta I = I_p - I_n = 2C\frac{\mathrm{d}V}{\mathrm{d}t}$, was used as an indicator of the capacitive component, as illustrated in Fig. S3[27]. For symmetry analysis, the *I*-*V* curves from the third cycle were used.

Results and discussion

The image flicker in the FFS mode at low-refresh rates, due to flexoelectric polarization coupling with the FFS electric field formation, has been extensively analyzed and addressed in previous reports[21,23–26]. In the FFS mode at normal mode (driving frequency > 30 Hz) as shown in Fig. 1(a, b), LC director reorients along the application of electric fields. Depending on the electrode position, dielectric coupling between LC and electric field changes the vectorial formation. These splay and bend deformations result in temporarily asymmetric LC director configuration in odd and even frames in which the driving frequency of the electric fields is set (in general) below 30 Hz, causing transmittance differences between frames that appear as flickers as shown in Fig. 1(c–f)[8,22,30].

When the flexoelectric effect is not considered in simulations using a finite element method (FEM) solver[23], there is no transmittance difference between frames, resulting in same space-dependent transmittance as shown in Fig. 1(b). However, when the flexoelectric effect is incorporated into FEM simulations, transmittance differences between even and odd frames emerge depending on the electrode position, as illustrated in Fig. 1(c). In odd frames, the transmittance decreases in regions over the patterned electrode branches and increases in the spaces between them. Conversely, in even frames, the transmittance increases over the electrode branches and decreases in the space between them.

Although the spatially integrated transmittance between frames depends on the scale of the patterned electrodes, transmittance fluctuations across frames caused by the flexoelectric effect in the FFS mode persist consistently. The AC frame-dependent formation of the electrical potential influences LC reorientation through dielectric and flexoelectric coupling. This suppresses splay deformation in regions where transmittance fluctuates, leading to increased twist deformation, which compensates for free energetic cost of the suppressed splay deformation. Consequently, transmittance differences between frames arise, potentially causing flicker in displays.

Experimental observations align with this finding, as polarizing optical microscopy (POM) images reveal significant space- (Fig. 1(d)) and time-dependent (Fig. 1(e, f)) transmittance deviations across electrode locations, confirming these brightness fluctuations over time. When low-frequency voltage is applied, the brightness fluctuates between the odd and even frames. This flickering effect can be easily verified by examining the time-dependent transmittance curves experimentally and numerically as shown in Fig. 1(e, f). From Fig. 1(e, f), we verified the flexoelectric coupling occurs near 30 Hz.

To design and develop the LC mixture for low contribution of flexoelectric effect in pLC, we verified the

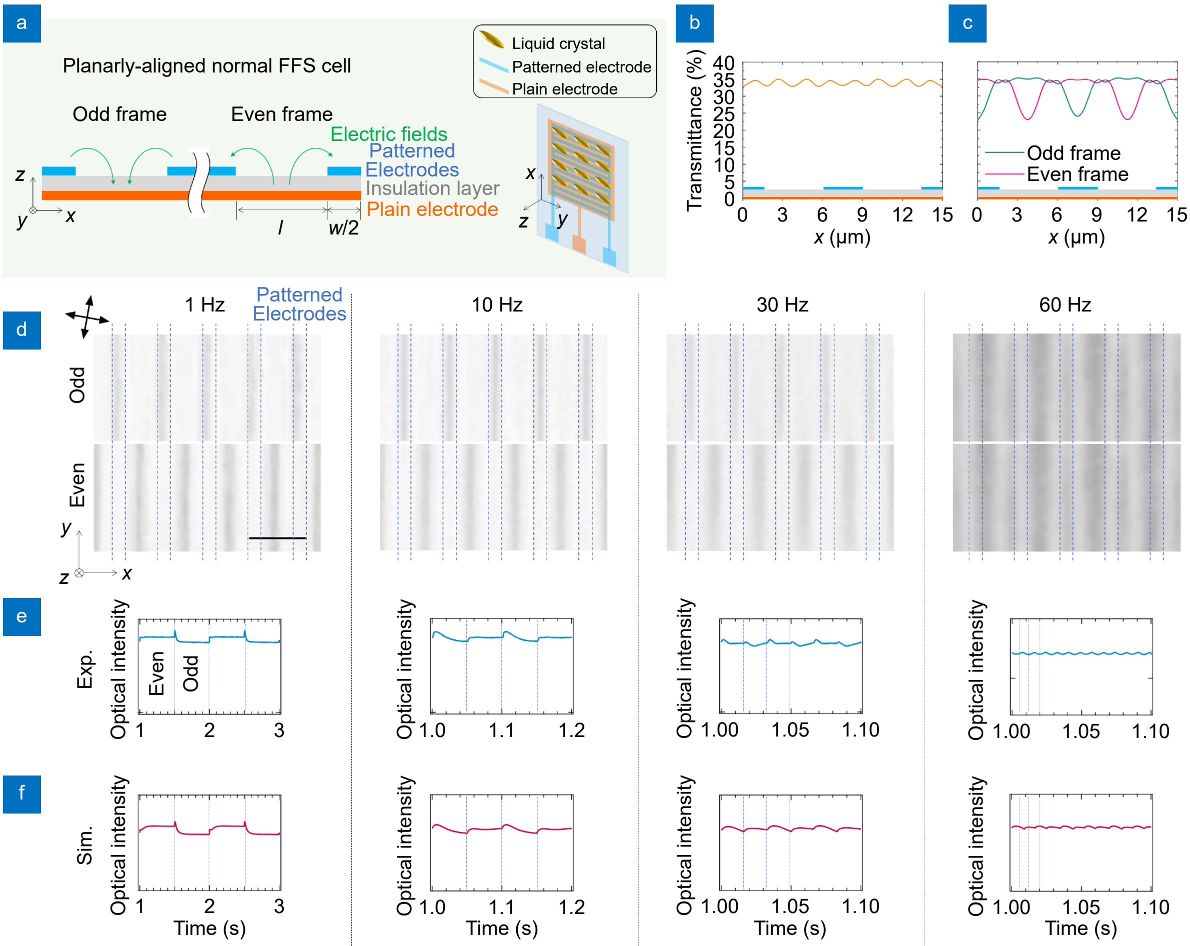

Fig. 1 | Flexoelectric effect appearing in an FFS mode with a positive LC (pLC0, applied voltage V = 6.2 V). (**a**) Schematic representation of the electric field formation in each AC frame based on the FFS electrode structure. The LC is homogeneously, planarly aligned in an FFS cell. (**b**, **c**) Simulated spatial transmittance from the FFS mode in (b) no flexoelectric and (c) flexoelectric mode using a FEM solver. (**d**) POM images of optical appearance of the flexoelectric effect in an FFS cell and (**e**, **f**) the time-dependent transmittance curves, obtained from experimental measurement and simulation when applying AC voltage at 1, 10, 30, 60 Hz. The black crossed arrows represent the transmittance axes of a polarizer and analyzer, and the scale bar is 10 μm in (d).

mechanism behind the phenomenon of flexoelectric effect. Figure 2(a, b) show common illustration of the molecular shapes for the understanding of the splay and bend flexoelectric polarizations. Assuming dipole moment (dark arrows) of each shape, when the dipole moments orient along one direction, the net polarization becomes non-zero. With dipole moment considering ideal positive dielectric anisotropy, bend deformation does not coincide with the flexoelectric polarization which the polarization direction perpendicular to the long axis of molecules. In this configuration, splay deformation is more suitable for the contribution to the flexoelectric polarization (purple arrows) than bend deformation as illustrated in Fig. 2(c). As described in Fig. 2(c), we can assume that in positive dielectric anisotropy LC, splay deformation significantly influences flexoelectric effects, leading to issues like flicker caused increased flexoelectric effect from LC mixtures composed of high polar constituents. Therefore, our goal was to optimize LC materials that minimize flexoelectric effects, focusing on LC mixtures that have mid-polar or low-polar characteristics. As shown in Table 1, we developed three LC materials with distinct properties (pLC1, pLC2, pLC3) and evaluated how flexoelectric effects arise and the differences between these new LC materials using newly developed measurement methods.

To verify the flexoelectric effect in the developed pLCs, we conducted simulations using a FEM solver alongside experimental measurements for the flexoelectric coefficient difference measurement as illustrated in Fig. 3(a). Notably, we adapted a newly developed measurement method originally designed for nLCs to assess

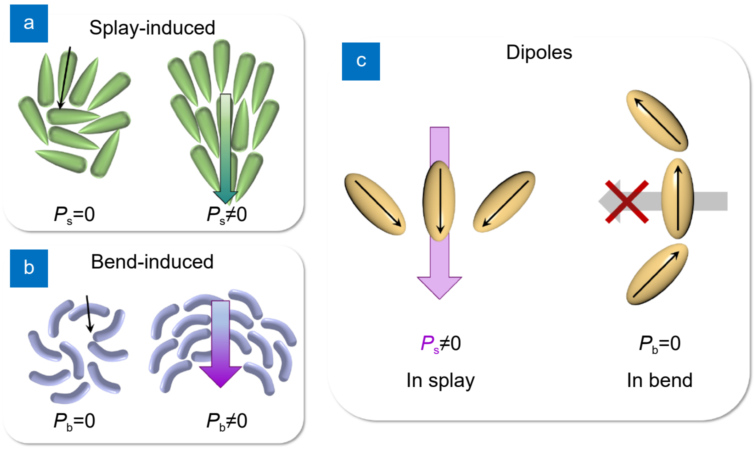

Fig. 2 | Illustration of molecular shapes for flexoelectric polarization. (**a**–**c**) Schematics of flexoelectric polarization P_s and P_b in splay and bend deformations for (a) pear- and (b) banana-shaped molecules, and (c) dipoles considering ideal positive dielectric anisotropy.

pLCs. This method utilizes a vertical alignment configuration with an FFS electrode structure, as illustrated in Fig. 3(b), to minimize measurement errors arising from factors such as ion impurity effects, which impact the voltage holding ratio (VHR)[31,32], and variations in surface anchoring strengths commonly observed with hybrid-aligned cells[33]. The proposed approach offers significant advantages, including the elimination of twist

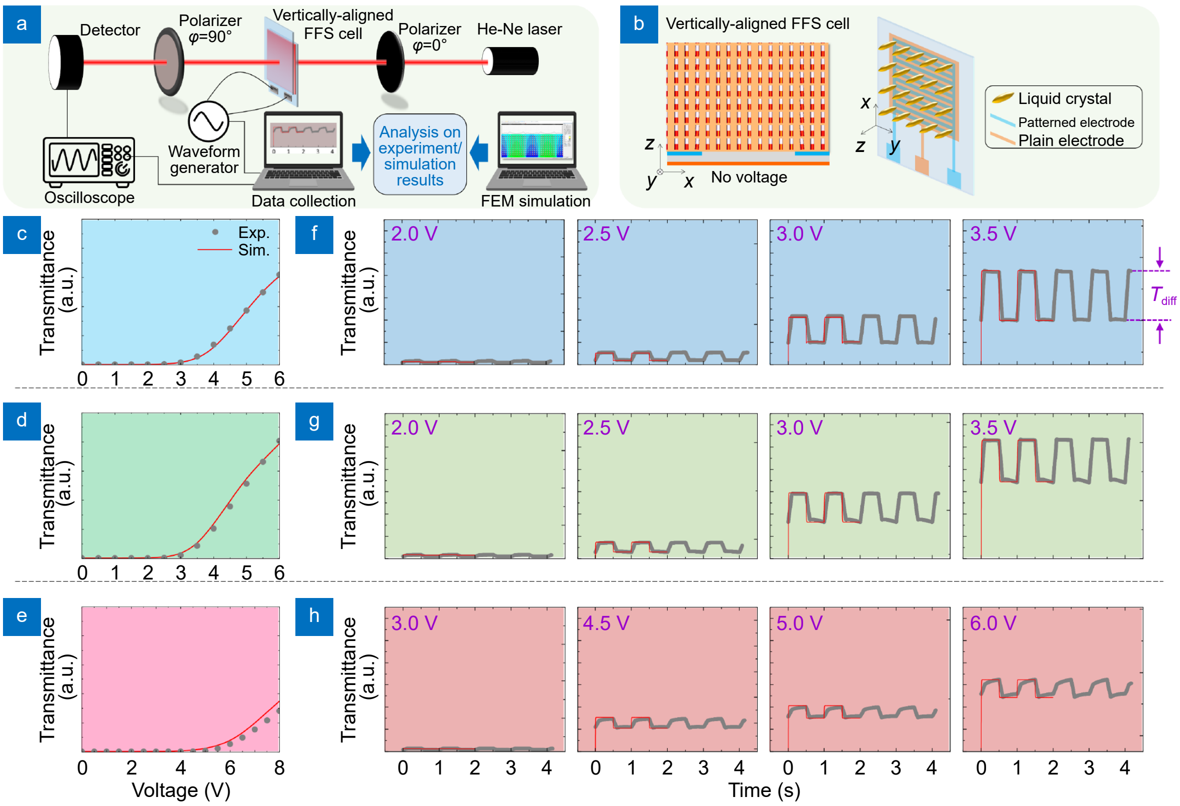

Fig. 3 | Experimental and simulated results for FFS cells incorporating pLC1–3. (**a**) Schematic of the optical setup used to measure transmittance differences related to the flexoelectric coefficient difference, with analysis comparing experimental and FEM simulation results. (**b**) Vertically aligned liquid crystal director configuration in the FFS cell, highlighting the conditions for evaluating flexoelectric coefficient differences. (**c**–**e**) Voltage-dependent transmittance curves measured at 1 kHz, where flexoelectric contributions are negligible. (**f**–**h**) Time-dependent transmittance curves measured at 1 Hz, where flexoelectric effects are pronounced. Data are shown for (c, f) pLC1, (d, g) pLC2, and (e, h) pLC3, respectively, for both experimental measurements and FEM simulations. The purple arrows in (e) indicate the transmittance difference T_{diff} between alternating frames under AC voltage conditions.

deformation in LC molecules and discrepancies in anchoring energy across alignment layers, thereby enhancing measurement accuracy and reliability. Importantly, this system facilitates the measurement of flexoelectric coefficient difference (e_s – e_b) in both pLCs and nLCs under identical electrode structural conditions, enabling direct and reliable comparisons between the two. Rather than merely extending prior methodologies, this study aims to validate the mechanism of flexoelectric contributions in pLCs.

The transmittance difference T_{diff} is determined by the stable transmittance in each frame after the frame transient moment (mostly within the LC response time τ < 50 ms). The transmittance difference is primarily attributed to the flexoelectric contribution and flickers. We conducted the FEM simulation and the measurement of voltage- (Fig. 3(c–e)) and time-dependent transmittance (Fig. 3(f–h)) with different LCs (pLC1, pLC2, pLC3) in a vertically aligned FFS cell to derive the flexoelectric coefficient difference under cross-validation. In Fig. 3(f–h), we measured the time-dependent transmittance for each liquid crystal and performed FEM simulations within the same structure to match the experimental results. We obtained time-dependent transmittance at various voltages at 1 Hz, observing that the transmittance difference $T_{diff} = T_{odd} - T_{even}$. When the transmittance difference T_{diff} converges to minimum values, flicker disappears, indicating that the flexoelectric effect is minimized, and (e_s – e_b) can be inferred based on T_{diff}. Based on the results shown in Fig. 3, we obtained the T_{diff} is reduced in the order of pLC1, pLC2, and pLC3, suggesting that (e_s – e_b) and flicker caused by flexoelectric effect are likely the smallest for pLC3.

The results in Fig. 4(a–c) include the spatial transmittance profiles (1st row), POM-like images (2nd row), and LC director fields (3rd row) using the FEM simulation, which confirmed that each LC exhibits a different transmittance between frames. The LC director configuration in each frame provides the detailed mechanism of flexoelectric contribution in splay and bend deformations. In pLC, we found that the splay deformation is mainly involved in differences in transmittance between odd and even frames. Based on the LC director contribution to the flexoelectric effect shown in Fig. 2(c), we analyzed the flexoelectric effect in pLCs through constructive and destructive coupling between electric fields and LC director, like our approach for nLCs (Fig. 4(e)).

To explain this in more detail, we separately illustrated the contributions of splay and bend flexoelectric polarizations to the constructive and destructive couplings in Fig. 4(d). In the odd frame, assuming splay deformation, the splay flexoelectric coupling is destructive because the vertical components of the splay polarization and electric field are in opposite directions. Conversely, in the second column, the vertical component of the electric field is inverted, making the splay flexoelectric coupling constructive in this region. Assuming bend deformation under the same electric field formation, as shown in the third column, the bend flexoelectric coupling is constructive because the bend flexoelectric polarization and the lateral component of the electric field are in the same direction. In the fourth column, the bending flexoelectric coupling is destructive because the lateral component of the bending flexoelectric polarization is reversed. Similarly, the splay and bend flexoelectric couplings can be illustrated in the even frame.

This analysis shows that if the polarity P_b due to bend deformation and the polarity P_s generated by splay deformation are similar or identical, the transmittance difference between odd and even frames can be minimized. That is, if (e_s – e_b) converges to zero, the splay and bend flexoelectric couplings would largely cancel each other out, reducing the overall flexoelectric contribution in terms of the system's free energy. This suggests that, as with nLCs, minimizing (e_s – e_b) in pLCs could serve as a basis for minimizing flicker. In vertically aligned cells as schematically illustrated in Fig. 3(a), (e_s – e_b) can be minimized in both pLCs (Fig. 4(d)) and nLCs (Fig. 4(e)) through the same mechanism without involving twist deformation, allowing flicker to be more predictably managed.

To verify that pLC3 exhibits the smallest flexoelectric effect, as predicted through both experiments and simulations in vertically aligned FFS cells in Fig. 3, we conducted measurements of the (e_s – e_b) as shown in Fig. 5. In Fig. 5(a–c), the measured (e_s – e_b) of three new pLCs (pLC1-3) is presented in Table 1. After obtaining T_{diff} with respect to the applied voltage, we conducted an FEM simulation and extracted T_{diff} values for various e_s and e_b values as shown in Fig. 5(a–c). The measured values were in good agreement with the voltage-dependent T_{diff} curves for pLC1 (e_s – e_b = 2.5), pLC2 (2.0), and pLC3 (0.5). Based on the consistent data between the FEM simulation and the actual experimental values, we measured the T_{diff} at 1 Hz driving conditions on the horizontally aligned normal FFS cells for each LC as shown

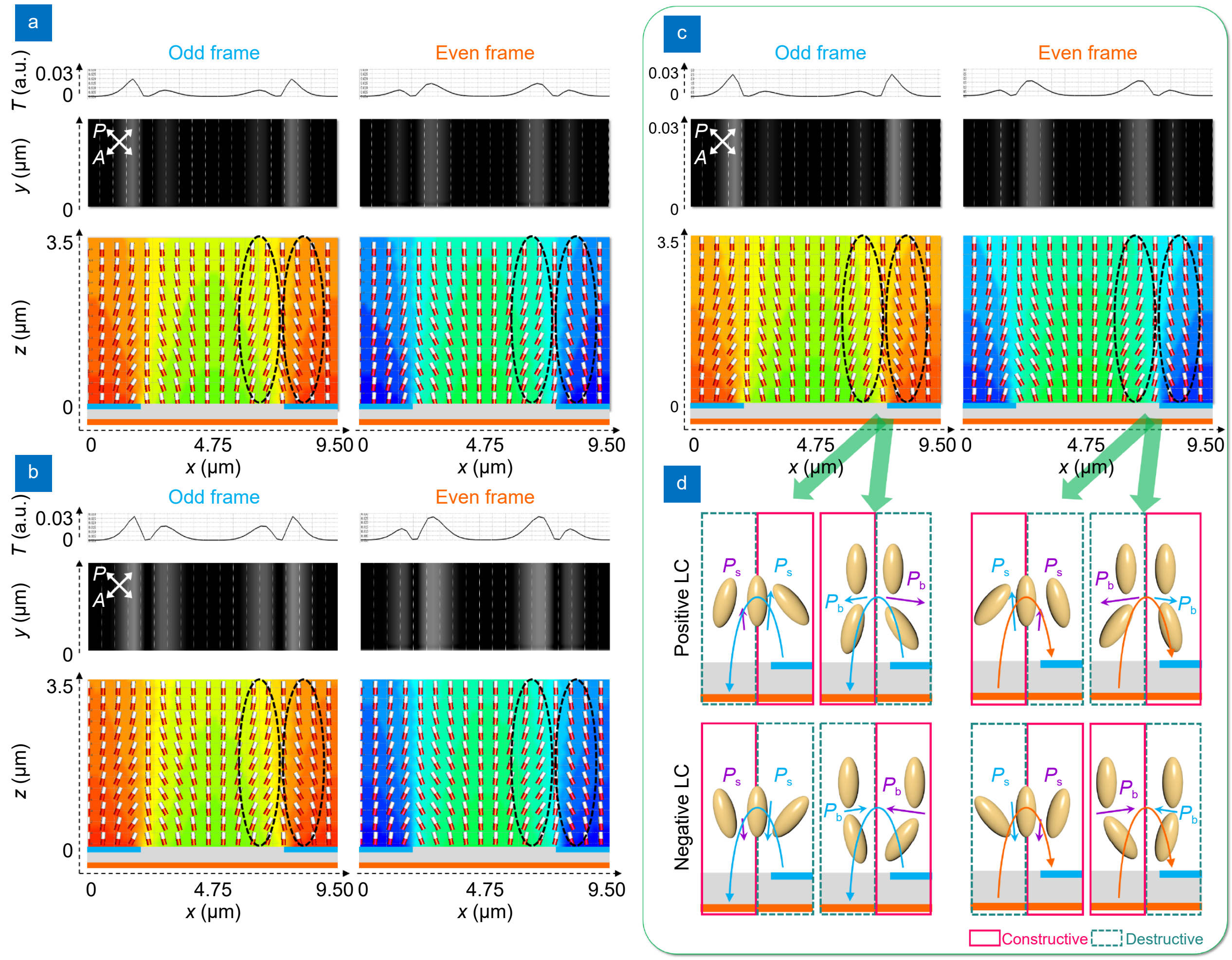

Fig. 4 | Vertically aligned FFS cells for the practical measurement of flexoelectric coefficient difference ($e_s - e_b$). (**a–c**) The spatial transmittance profiles (1st row), POM-like images (2nd row) and LC director fields (3rd row) of (a) pLC1 (V = 3.5 V), (b) pLC2 (V = 3.5 V) and (c) pLC3 (V = 5.5 V). (**d**, **e**) Analysis of flexoelectric coupling in the flexoelectric coefficients measurement system. The contributions of splay and bend flexoelectric polarizations to both constructive and destructive couplings[21] in different positions within the FFS cell at certain voltage for (d) a pLC and (e) an nLC.

in Fig. 5(d). The results indicate that (e_s – e_b) of the experiment and FEM simulation on vertically aligned FFS cell closely matches the actual T_{diff} on a real FFS cell, demonstrating that (e_s – e_b) is highly correlated with flicker in a real FFS cell. From these findings, we conclude that minimizing the (e_s – e_b) is crucial, and this result is both encouraging and meaningful from an engineering perspective.

In the DCM method, as illustrated in Figs. 6(a) and S2, a triangular voltage waveform is applied to the test cells. The voltage amplitude varies linearly over time, while the resulting current is measured[27]. The LC cells are electrically modeled as a parallel combination of a resistor and a capacitor, as depicted in the equivalent circuit in Fig. S2. DCM results for pLC1 (Fig. 6(c, f)), pLC2 (Fig. 6(d, g)), and pLC3 (Fig. 6(e, h)) in VA-FFS cells are presented for two AC driving frequencies: 0.1 Hz (Fig. 6(b–d)) and 0.01 Hz (Fig. 6(e–g)). Under applied voltage, the LC directors reorient similarly to the configuration illustrated in Fig. 4(d), following the voltage cycle: $V = 0$, $V > 0$ (odd frame), $V = 0$, $V < 0$ (even frame), and returning to $V = 0$, as shown schematically in Fig. 6(h). As detailed in the Section *Experimental* and Fig. S2, the capacitance C is proportional to the current difference ΔI, which reflects the capacitive response during LC reorientation. When the applied voltage exceeds the threshold voltage ($V > V_{th}$), ΔI changes slightly due to the realignment of LC molecules between the patterned (blue rectangle) and planar (orange rectangle) electrodes, influenced by the generated electric field (Fig. 6(h)).

As the driving frequency decreases from 0.1 Hz to 0.01 Hz, ΔI also decreases, as seen in Fig. 6(f–h). At lower

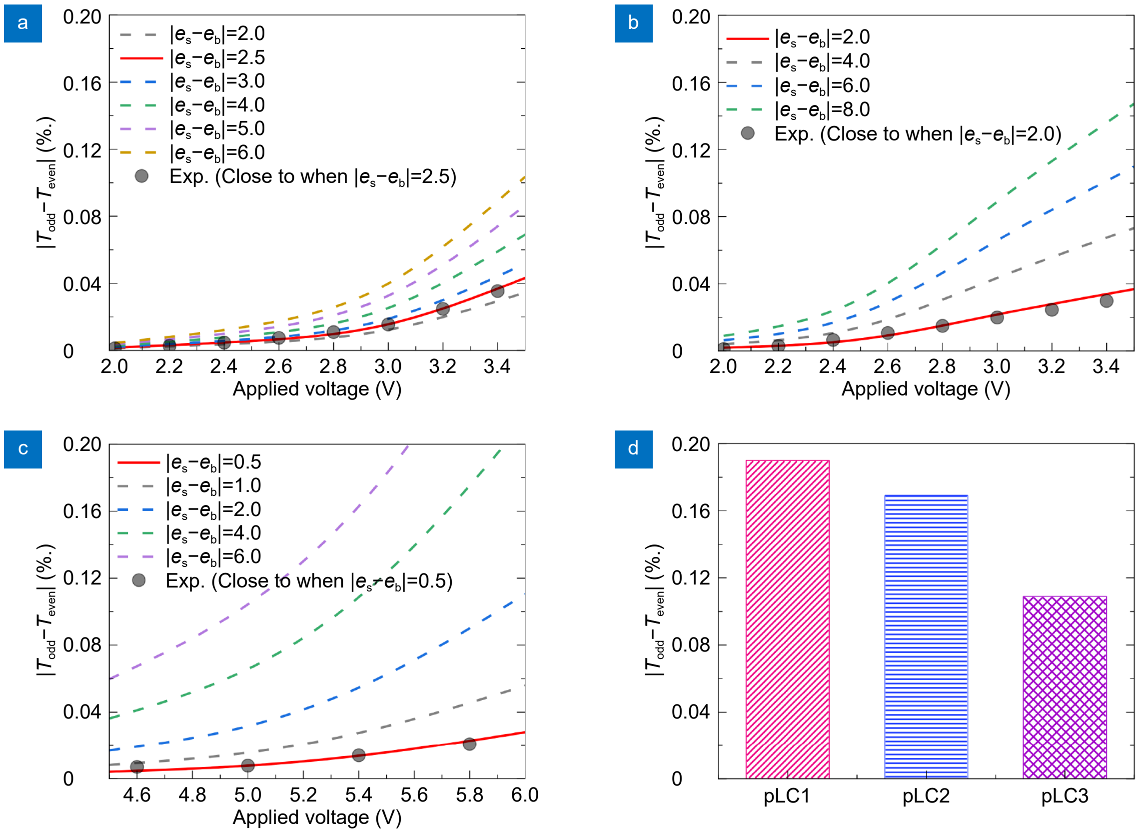

Fig. 5 | The measurement and analysis of the flexoelectric coefficient difference (e_s – e_b) of the *vertically* aligned FFS (VA-FFS) cells and verification using planarly aligned normal FFS cells. (**a**) pLC1, (**b**) pLC2, (**c**) pLC3 in VA-FFS cells. (**d**) Transmittance difference (at $T_{50\%}$) for pLC1 (V = 2.5 V), pLC2 (V = 2.4 V), and pLC3 (V = 3.6 V) in the planarly aligned normal FFS cells.

frequencies, the influence of ionic motion and LC reorientation on the *I*-*V* characteristics becomes more pronounced. While the symmetry in general LC switching behavior (i.e., in the normal dielectric mode) remains consistent across all pLC samples, deviations caused by flexoelectric effects become evident in the *I*-*V* curves through the breaking of symmetry about the voltage and current axes. When the flexoelectric contribution is substantial, the LC configurations at $V > 0$ and $V < 0$ diverge, resulting in asymmetric *I*-*V* responses. To quantify this asymmetry, the *I*-*V* curve in the third quadrant was mirrored to compare against the first quadrant, as shown in Fig. 6(i–k). At 0.1 Hz, all pLCs exhibit some degree of asymmetry, highlighted as the pink-shaded regions representing the current difference. These differences were averaged and plotted in Fig. 6(l). Among the samples, pLC3 exhibited the smallest current difference, indicating the weakest flexoelectric response. pLC2 showed a slightly lower current difference than pLC1, consistent with the transmittance difference results presented in Fig. 5. As the frequency decreased further, the same trend in current difference was observed, although the effect became less distinct due to increasing contributions from ionic conduction. These results collectively indicate that a smaller current difference between the first and third quadrants corresponds to a smaller transmittance difference, signifying minimized deviation in the flexoelectric effect between odd and even frames.

A comparison between the transmittance difference and the current difference reveals consistent trends under applied electric fields, reflecting similar LC deformation behavior. As shown in Fig. 4, slight tilting of the LC directors in response to the electric field leads to an increase in brightness, which differs between odd and even frames due to the flexoelectric effect. These director tilts similarly result in measurable differences in current between the frames. In particular, when the splay flexoelectric contribution becomes dominant in pLCs, the flexoelectric coefficient difference (e_s – e_b) and the corresponding current difference increase significantly—correlating with the severity of display flicker. Although these results may not directly prescribe specific molecular structures, they provide a reliable and accessible method for quantifying the flexoelectric coefficient

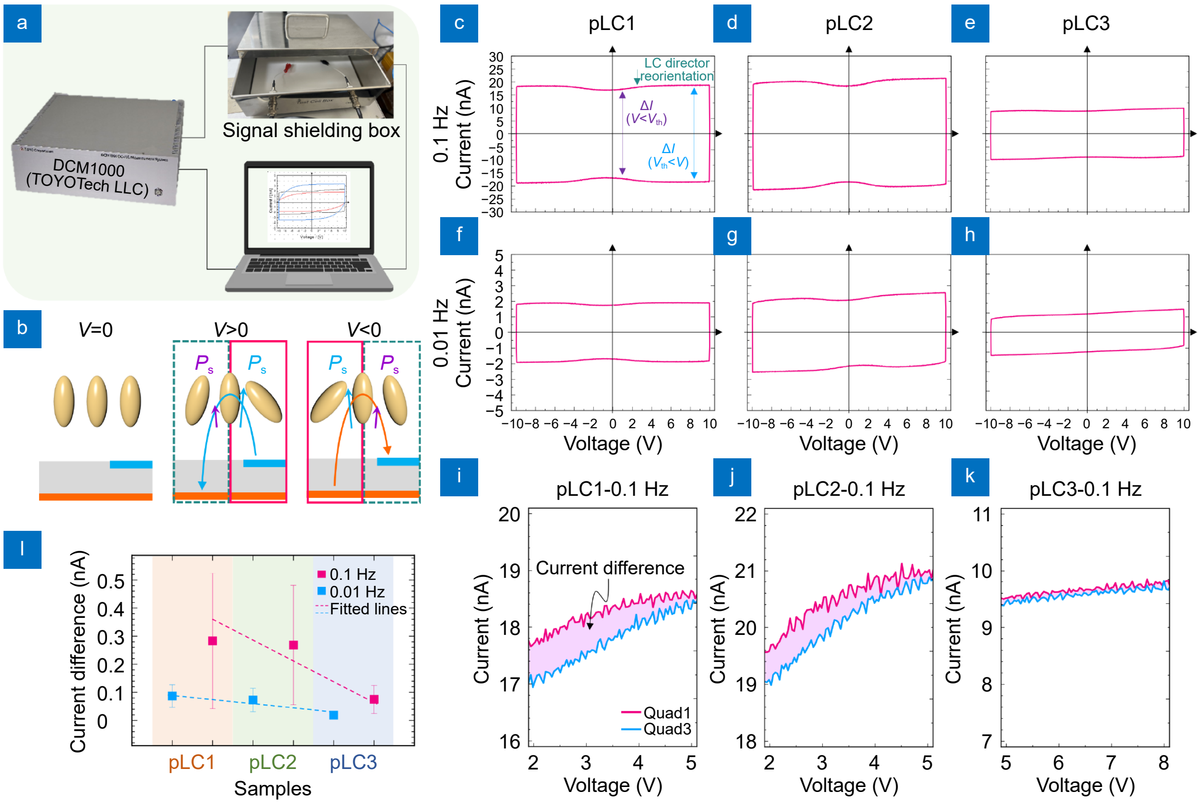

Fig. 6 | Displacement-current measurement (DCM) results for pLC1, pLC2, and pLC3. (**a**) Schematic of the DCM setup using commercial instrumentation equipped with an electromagnetic shielding box for the test cells and integrated analysis software. (**b**) Schematic illustration of LC director orientations during voltage transitions: $V = 0$, $V > 0$, and $V < 0$. (**c–h**) Measured current–voltage (I–V) curves at AC driving frequencies of 0.1 Hz (c–e) and 0.01 Hz (f–h) for vertically aligned FFS cells filled with (c, f) pLC1, (d, g) pLC2, and (e, h) pLC3. These are the same cells used to evaluate the flexoelectric coefficient difference ($e_s - e_b$) through brightness measurements. (**i–k**) Symmetry analysis of the I–V curves in (**c–e**), comparing the absolute current values between the first and third quadrants to evaluate flexoelectric asymmetry. (**l**) Averaged current differences for pLC1–3 extracted from (**i–k**), with fitted trends indicated by red- and blue-dotted lines.

difference. The strong agreement between both measurement approaches (brightness and current difference) supports the feasibility of using them to guide molecular design strategies, particularly those aimed at minimizing the splay flexoelectric coefficient e_s in pLCs.

Conclusions

Positive dielectric anisotropy liquid crystals (pLCs) have traditionally been excluded from low-frequency driving technologies aimed at reducing power consumption, primarily due to their susceptibility to significant splay deformation in fringe-field switching (FFS) mode of liquid crystal displays. This deformation exacerbates flicker performance through the flexoelectric effect, making them less favorable compared to negative dielectric anisotropy liquid crystals (nLCs). However, nLCs inherently exhibit high driving voltages and a limited range of single LC combinations, which often fail to meet product performance requirements. In contrast, pLCs offer inherently lower driving voltages and greater flexibility in single LC combinations, enabling the development of a wide range of LCs with diverse performance characteristics.

In this study, we introduced a novel methodology for predicting the flexoelectric coefficient difference ($e_s - e_b$) in pLCs by analyzing the molecular-level contributions to the flexoelectric effect. Through a combination of FEM simulations and experimental measurements, we validated an optical approach that quantifies this coefficient difference as a proving parameter governing flicker performance. Additionally, we proposed and implemented a DCM technique to independently assess and confirm the flexoelectric response. Both methods exhibited strong consistency in evaluating the flexoelectric contribution and its influence on flicker behavior.

Our results show that reducing molecular asymmetry and electrical polarity within the pLC mixtures effectively lowers the splay flexoelectric coefficient, which exerts a more pronounced influence on flicker than the bend coefficient in pLCs. We demonstrated that the flexoelectric coefficient difference can be accurately measured using VA-FFS cells. This configuration eliminates twist deformation, enabling a direct correlation between LC deformation and optical performance.

The proposed transmittance difference measurement system significantly simplifies the analysis by avoiding the complexities and ambiguities associated with conventional methods. Furthermore, the DCM technique—implemented using a commercially available system —offers a streamlined and user-friendly experimental protocol. By analyzing the current symmetry in the *I*-*V* characteristics, the DCM method provides a straightforward means to verify the flexoelectric effect, further supporting its practical application in evaluating flicker performance.

This advancement holds substantial potential for the display industry, as pLCs inherently provide higher reliability, lower production costs, and a broader range of single LC candidates compared to nLCs. By enabling the development of pLCs with minimized splay flexoelectric coefficient while preserving key electro-optic properties such as low driving voltage and fast response times, we believe this work paves the way for the development of superior low-power displays with advanced performance characteristics.

References

1. Appliances and equipment – Analysis - IEA. https://www.iea.org/reports/appliances-and-equipment.
2. Mansouri I, Newborough M, Probert D. Energy consumption in UK households: impact of domestic electrical appliances. *Appl Energy* **54**, 211–285 (1996).
3. Kim DS, Kwon OK. A new dot inversion data addressing technique using double rate driving method for high image quality and low-power TFT-LCDs. *J Display Technol* **12**, 1019–1026 (2016).
4. Lin FC, Huang YP, Liao LY et al. Dynamic backlight gamma on high dynamic range LCD TVs. *J Display Technol* **4**, 139–146 (2008).
5. Gatti F, Acquaviva A, Benini L et al. Low power control techniques for TFT LCD displays. In *Proceedings of the 2002 International Conference on Compilers, Architecture, and Synthesis for Embedded Systems* 218–224 (Association for Computing Machinery, 2002). https://doi.org/10.1145/581630.581664.
6. Kim MS, Lee SL, Lee SH. Fringe-field switching technology. In Ishihara S, Kobayashi S, Ukai Y. *High Quality Liquid Crystal Displays and Smart Devices - Volume 1: Development, Display Applications and Components* 55–77 (Institution of Engineering and Technology, 2019). doi: 10.1049/PBCS068F_ch3.
7. Kim MS, Ham HG, Choi HS et al. Flexoelectric in-plane switching (IPS) mode with ultra-high-transmittance, low-voltage, low-frequency, and a flicker-free image. *Opt Express* **25**, 5962–5971 (2017).
8. Kim MS, Jin HS, Lee SJ et al. Liquid crystals for superior electro-optic performance display device with power-saving mode. *Adv Opt Mater* **6**, 1800022 (2018).
9. Meyer RB. Piezoelectric effects in liquid crystals. *Phys Rev Lett* **22**, 918–921 (1969).
10. Tagantsev AK. Piezoelectricity and flexoelectricity in crystalline dielectrics. *Phys Rev B* **34**, 5883–5889 (1986).
11. Buka Á, Éber N. *Flexoelectricity in Liquid Crystals: Theory, Experiments and Applications* (Imperial College Press, London, 2013).
12. Lee DJ, Jung JH, Shin JS et al. 13-1: *invited paper*: liquid crystal display optimized for gaming applications and future. *SID Symp Dig Technic Pap* **50**, 160–163 (2019).
13. Jung J, Park HB, Jung HY et al. Recent progress in liquid crystal devices and materials of TFT-LCDs. *J Inf Display* **25**, 121–142 (2024).
14. Lee SH, Bhattacharyya SS, Jin HS et al. Devices and materials for high-performance mobile liquid crystal displays. *J Mater Chem* **22**, 11893–11903 (2012).
15. Fernández MR, Casanova EZ, Alonso IG. Review of display technologies focusing on power consumption. *Sustainability* **7**, 10854–10875 (2015).
16. Deng MY, Hsiang EL, Yang Q et al. Reducing power consumption of active-matrix mini-LED backlit LCDs by driving circuit. *IEEE Trans Electron Dev* **68**, 2347–2354 (2021).
17. Lee SH, Lee SL, Kim HY. Electro-optic characteristics and switching principle of a nematic liquid crystal cell controlled by fringe-field switching. *Appl Phys Lett* **73**, 2881–2883 (1998).
18. Kim HY, Hong SH, Park TK et al. Electrooptic characteristics of the fringe-field switching device with electrode on top substrate. *Jpn J Appl Phys* **41**, 176–181 (2002).
19. Jung JH, Ha KS, Chae M et al. Light efficiency of the dependence of fringe-field switching mode on the of the dielectric anisotropy of liquid crystal for various values of the cell gap and the rubbing angle. *J Korean Phys Soc* **56**, 548–553 (2010).
20. Kim MS, Lee DY, Park HB et al. Ultralow power consumption liquid crystal display retaining superior image qualities. *Adv Opt Mater* **12**, 2301963 (2024).
21. Kim MS, Bos PJ, Kim DW et al. Flexoelectric effect in an in-plane switching (IPS) liquid crystal cell for low-power consump-
22. tion display devices. *Sci Rep* **6**, 35254 (2016).
23. Kim MS, Bos PJ, Kim DW et al. Field-symmetrization to solve luminance deviation between frames in a low-frequency-driven fringe-field switching liquid crystal cell. *Opt Express* **24**, 29568–29576 (2016).
24. Lee H, Kim H, Kim J et al. Dependence of image flickering of negative dielectric anisotropy liquid crystal on the flexoelectric coefficient ratio and the interdigitated electrode structure. *J Phys D Appl Phys* **49**, 075501 (2016).
25. Choi JC, Lee JW, Lee DJ et al. Flicker-free fringe-field switching liquid crystal display operable at extremely low frequencies for power saving. *Adv Eng Mater* **23**, 2100174 (2021).
26. Oh SW, Park JH, Lee JH et al. Elimination of image flicker in a fringe-field switching liquid crystal display by applying a bipolar voltage wave. *Opt Express* **23**, 24013–24018 (2015).
27. Inoue M, Oyabu N, Kaneko Y et al. Correlation between ion impurity in thermally activated delayed fluorescence organic light-

emitting diode materials and device lifetime. *J Soc Inf Disp* **28**, 905–910 (2020).

28. Helfreich W. The strength of piezoelectricity in liquid crystals. *Z Naturforsch A* **26**, 833–835 (1971).
29. Helfrich W. A simple method to observe the piezoelectricity of liquid crystals. *Phys Lett A* **35**, 393–394 (1971).
30. Davis J, Hsieh YH, Lee HC. Humans perceive flicker artifacts at 500 Hz. *Sci Rep* **5**, 7861 (2015).
31. Lee TR, Kim JH, Lee SH et al. Investigation on newly designed low resistivity polyimide-type alignment layer for reducing DC image sticking of in-plane switching liquid crystal display. *Liq Cryst* **44**, 738–747 (2017).
32. Toko Y, Sugiyama T, Katoh K et al. Amorphous twisted nematic–liquid - crystal displays fabricated by nonrubbing showing wide and uniform viewing - angle characteristics accompanying excellent voltage holding ratios. *J Appl Phys* **74**, 2071–2075 (1993).
33. Takahashi T, Hashidate S, Nishijou H et al. Novel measurement method for flexoelectric coefficients of nematic liquid crystals. *Jpn J Appl Phys* **37**, 1865–1869 (1998).

Acknowledgements

This work was supported by Basic Science Research Program through the National Research Foundation (NRF) of Korea, funded by the Ministry of Science and ICT (MSIT), Korea [2022R1A2C2091671]; and by ITECH R&D Program of MOTIE/KEIT (Ministry of Trade, Industry & Energy / Korea Evaluation Institute of Industrial Technology) [20016808]. The authors thank to Masaru Inoue for valuable comments on the DCM analysis.

Competing interests

The authors declare no competing financial interests.

Supplementary information

Supplementary information for this paper is available at https://doi.org/10.29026/oea.2025.250022

Scan for Article PDF